IEEJ Journal of Industry Applications
Vol.5 No.3 pp.206–214 DOI: 10.1541/ieejjia.5.206

Paper

Galvanic Isolation System with Wireless Power Transfer for Multiple Gate Driver Supplies of a Medium-voltage Inverter

Keisuke Kusaka[*] Student Member, Koji Orikawa[*] Member
Jun-ichi Itoh[*a)] Member, Isamu Hasegawa[**] Non-member
Kazunori Morita[**] Member, Takeshi Kondo[**] Non-member

(Manuscript received April 30, 2015, revised Sep. 12, 2015)

In this paper, a gate driver supply, which supplies power to multiple gate drivers, is demonstrated. Robust isolation is required in the gate drive supplies of a medium-voltage inverter in order to drive high-voltage switching devices such as insulated-gate bipolar transistors. The proposed isolation system achieves isolation with transmission coils mounted on printed circuit boards. Furthermore, the isolation system transmits power from one transmitting board to six receiving boards. In the conventional system, the number of receivers is limited to one. In contrast, multiple receivers are acceptable in the proposed system. These characteristics help reduce the of the isolation system for the gate driver supplies.

This paper presents the fundamental characteristics of the isolation system. The equivalent circuit of the proposed system can be derived by applying the equivalent circuit of a wireless power transfer system with a repeater coil. In addtion, a design method for the resonance capacitors is mathematically introduced using the equivalent circuit. It is verified that an isolation system with multiple receivers can be designed using the same resonance conditions as an isolation system with a single receiver.

Moreover, the isolation system is experimentally demonstrated. It is confirmed that the isolation system transmits power with a maximum efficiency of 46.9% at an output power of 16.6 W beyond an air gap of 50 mm with only printed circuit boards.

Keywords: wireless power transfer, inductive coupling, isolation, medium-voltage inverter, gate driver

1. Introduction

In recent years, the system voltage of a three-phase medium-voltage inverter for industrial applications has risen to 3.3 kV or 6.6 kV [(1)–(5)]. In a medium-voltage inverter, galvanic isolation is required at each gate driver supply. The standards of isolation, which are published by the International Electrotechnical Commission (IEC), are well-known safety regulations. For example, the safety standards of the IEC require a minimum clearance of 14 mm and a creepage distance of 81 mm under the following conditions: the working voltage of the inverter is 8.0 kV, and the comparative tracking index (CTI) is $100 \leq \mathrm{CTI} < 400$ with a pollution degree of 2 [(6)]. In general, isolation transformers with cores are commonly used for isolation. However, they cause an increase in cost because isolation transformers are typically custom built. In addition, the isolation transformer is large in order to obtain a high isolation voltage. For example, the typical dimensions of the isolation transformer, which has an isolation voltage of 20 $\mathrm{kV_{rms}}$ for 10 s, are 200 mm × 200 mm × 200 mm at a weight of approximately 5.5 kg [(7)]. These transformers must be placed at each of the gate driver supplies.

In order to achieve the cost reduction and downsizing of the isolation system, a single-chip DC-isolated gate drive integrated circuit (IC) has been proposed [(8)–(10)]. It supplies power using a microwave from the bottom layer of a sapphire substrate to the top layer. In this method, the sapphire substrate assumes galvanic isolation. It can significantly downsize the isolation system. However, it does not satisfy the safety standards of the medium-voltage inverter because the creepage distance is not enough.

In (11), galvanic isolation is assumed by an optical fiber. The power for a gate drive is supplied through an optical fiber. However, the transmitted power is limited to 100 mW per one fiber.

Meanwhile, J.W. Kolar et al. have proposed an isolation system using printed circuit boards (PCBs) [(12)]. It achieves galvanic isolation with a coreless transformer. However, one transmitting side transmits power to only one receiving side one-by-one (1 × 1) in this system. Thus, isolation systems are also required at each gate driver supply. Therefore a number of isolation systems are required in order to supply power. This prevents the downsizing of isolation systems.

a) Correspondence to: Jun-ichi Itoh. E-mail: itoh@vos.nagaokaut.ac.jp
[*] Nagaoka University of Technology
1603-1, Kamitomioka-machi, Nagaoka, Niigata 940-2188, Japan
[**] MEIDENSHA CORPORATION
515, Kaminakamizo, Higashimakado, Numazu, Shizuoka 410-8588, Japan

In this paper, the galvanic isolation system with multiple receivers is demonstrated and analyzed based on an equivalent circuit. The isolation system transmits power from one transmitting board to six receiving boards (1×6) beyond an air gap of 50 mm. The isolation system contributes to the cost reduction and downsizing of the isolation system. Moreover, the isolation with an air gap of 50-mm easily meets the standards for clearance and creepage distance when the system voltage of the inverter is 6.6 kV. Moreover, the 50 mm air gap decreases the common-mode current, which is induced by the high-dv/dt switching of a medium-voltage inverter.

This paper first describes the system configuration of the proposed isolation system. Secondly, the equivalent circuit of the wireless power transfer system with multiple PCBs is introduced. The validity of the equivalent circuit model is evaluated by comparing the F-matrix of the wireless power transfer system between the three-dimensional (3-D) electromagnetic analysis and the equivalent circuit model. Then, the evaluation of the equivalent circuit and the design method of resonance capacitors for efficient wireless power transfer are mathematically clarified. Finally, the experimental results are presented.

2. Proposed Isolation System

2.1 System Configuration Figure 1 shows the concept of the proposed isolation system for a medium-voltage inverter. The isolation system consists of one transmitting board and six receiving boards. The power consumption in the gate drivers is supplied through the isolation system from a low-voltage power supply of 24 V in a medium-voltage inverter.

Incidentally, a wireless power transfer system with a high quality factor Q of the transmission coils has been studied in recent years [13]–[17]. Wireless power transfer systems use resonance in order to compensate for leakage inductance because weak magnetic coupling causes a large leakage inductance [14]. Common techniques are used in the proposed system. In the conventional system, the transformer with a core prevents the cost reduction and downsizing of the isolation system. In contrast, the isolation system is constructed using only PCBs in this system. The PCBs can be manufactured easily and inexpensively in comparison with the transformer. This configuration contributes to a weight saving of the isolation system. The total weight of the isolation system for six gate drivers is approximately 890 g.

In the isolation system, a transmission frequency of 2.0 MHz is used because a high-frequency transmission is required in order to decrease the required inductance for resonance. Moreover, the operation at a high frequency above 2 MHz limits the selection of MOSFETs.

Figure 2 shows the positional relationship of the transmitting board and the receiving boards. The maximum size of the system is constrained up to 300 mm × 150 mm × 150 mm due to the space limitations of the medium-voltage inverter. The receiving boards are placed at the top and bottom of the transmitting board. Each distance between the receiving boards and the transmitting board is kept at a minimum of 50 mm for the galvanic isolation. It contributes a robust galvanic isolation and a low common-mode current through parasitic capacitances. It is enough to fulfill the safety standards

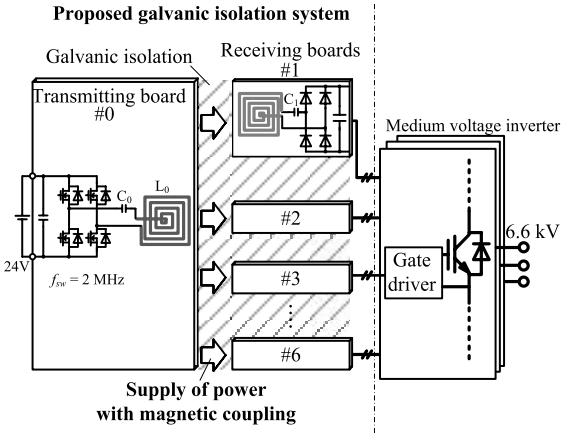

Fig. 1. Concept of the proposed isolation system

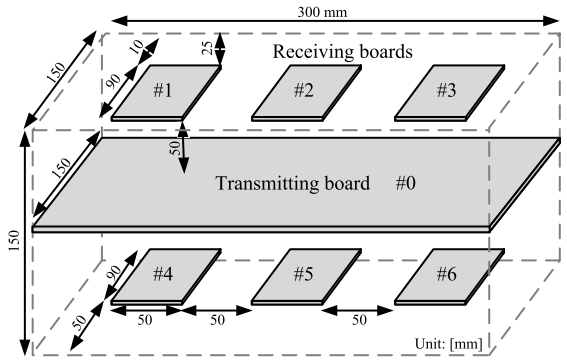

Fig. 2. Placement of the transmitting board and receiving boards. Each board is placed across an air gap of 50 mm

of the IEC [6] when the output voltage of the medium-voltage inverter is 6.6 kV. Note that an air gap of 50 mm contains a sufficient margin towards productization.

The number of receiving boards can be increased by expanding the transmission board. However, the expansion of the transmission board causes an increase of the equivalent series resistance of the transmission coil. It will decrease transmission efficiency. Besides, the greatest common denominator of the number of switches for three-phase inverters is six. Thus, six receiving boards are placed in this paper.

Figures 3 and 4 show the shapes of the transmitting coils and receiving coils, respectively. Transmitting board #0 consists of a high-frequency inverter, a series resonance capacitor, and a transmitting coil for a wireless power transfer system. The inverter is operated by a square wave operation with an output frequency of 2 MHz. On the other hand, receiving boards #1–6 consist of receiving coils, series resonance capacitors, and diode bridge rectifiers. The thickness of the copper film for both boards is 175 μm.

2.2 Evaluation of Parasitic Capacitance In this section, the parasitic capacitance between the transmitting board and the receiving boards is evaluated. The parasitic capacitances between the transmitting board and the receiving boards should be suppressed because parasitic capacitances reduce the isolation performance. The parasitic capacitances among the boards correspond to the capacitance between a primary winding and a secondary winding in a conventional isolation system with a transformer. In particular,

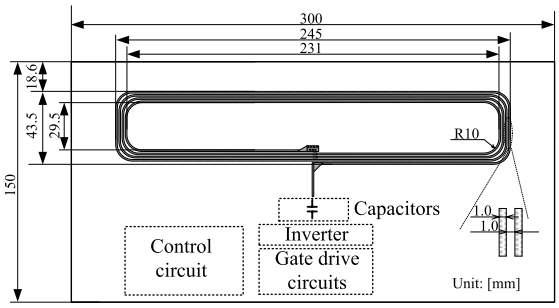

(a) Component side.

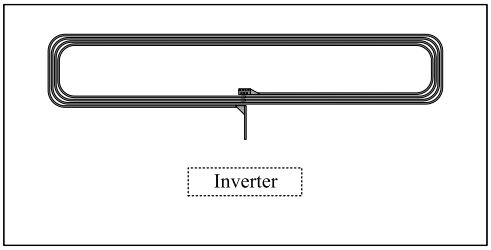

(b) Solder side.

Fig. 3. Schematics of the transmitting board

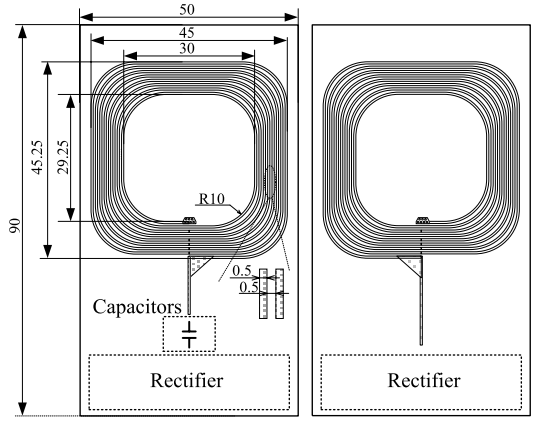

(a) Component side. (b) Solder side.

Fig. 4. Schematics of the receiving board

since the silicon carbide (SiC) MOSFETs have begun to be used in place of conventional Si-IGBT, suppression of the parasitic capacitance is important. A SiC-MOSFET will improve the efficiency of medium-voltage inverter because a SiC-MOSFET greatly improves the switching speed due to its high electronic mobility [18][19]. Thus, a large common-mode current caused by high dv/dt flows into the control circuit through the parasitic capacitance between the windings. The suppression of the parasitic capacitances is strongly required.

However, it is difficult to calculate the exact parasitic capacitance because the shapes of the conductors on the transmitting board and the receiving board are complicated. The measurement of the parasitic capacitances between the boards is also difficult since the parasitic capacitances are very small. Thus, the parasitic capacitance is analyzed by an electromagnetic analysis (Agilent, ADS) under the worst-case assumptions that both the transmitting board and the receiving board are covered with copper. The electromagnetic analysis shows that the parasitic capacitances between the transmitting board and the receiving boards with an air-gap of 50 mm are less than 4.4 pF. This shows that the proposed isolation system decreases the parasitic capacitance in comparison with the conventional isolation system with a transformer [20][21].

3. Analysis of Proposed Isolation System

In this section, this paper first presents the equivalent circuit of the multiple wireless power transfer system because the equivalent circuit is required in order to design the resonance capacitance to compensate for the leakage inductance. The validity of the equivalent circuit model is clarified by a comparison of the F-matrix between the equivalent circuit model and a 3-D electromagnetic analysis. According to the equivalent circuit, resonance capacitors that compensate for the leakage inductance are selected. It is shown that the resonance conditions are likewise given for the isolation system with one receiver.

3.1 Derivation of Equivalent Circuit The proposed system supplies power using a weak magnetic coupling from the transmitting coil to the each receiving coils. For this reason, a power factor from the view point of the output of the inverter is extremely low. In order to compensate the leakage inductance using resonances, series or parallel capacitors are commonly used in the research field about a wireless power transfer [14]. In this system, series-series compensation method is used. The resonance capacitors ($C_{0\text{–}6}$) are inserted in a series to the each coil. These resonance capacitors should be selected in order to cancel out a reactance from the view point of the output of the inverter. It means that the output power factor of the inverter should be unity.

Figure 5 shows the equivalent circuit of the isolation system where $L_{le0\text{–}6}$ are the leakage-inductances, $L_{m1\text{–}6}$ are the magnetizing inductances, k_{ij} is the coupling coefficient between boards #i and #j, $N_{0\text{–}6}$ are the numbers of turns, $r_{0\text{–}6}$ are the equivalent series resistances, and a is the turn ratio defined as $N_{1\text{–}6}/N_0$. The method of the derivation of the equivalent circuit is described in the next paragraph. The magnetic coupling among the receiving coils can be ignored because the magnetic coupling between the receiving coils, which are placed in side by side such as the boards #1 and #2, is approximately $k_{12} = 0.005$. The magnetic coupling between the coils #1 and #2 is three times smaller than the magnetic coupling between the coils #0 and #1.

Figures 6(a) and (b) show a schematic and the equivalent circuit of a wireless power transfer system with repeater coil [22], respectively, where $L_{A\text{–}C}$ are the self-inductances of each coil. The equivalent circuit of the proposed system shown in Fig. 5 is derived by applying the equivalent circuit of the repeater coil in (22)–(23). The repeater coil was invented in order to extend the transmission distance [22][23]. In the wireless power transfer system with a repeater coil, the power supply, which has the inner impedance Z_{01}, is connected to the coil A. The power is supplied to the coil C through the coil B because the coil B is magnetically coupled to both the coil A and coil B.

Figures 6(c) and (d) show the schematic and the equivalent circuit of a wireless power transfer system with multiple receivers, respectively. By interchanging the connection of the power supply from coil A to coil B in Fig. 6(b), the equivalent circuit of the wireless power transfer system with

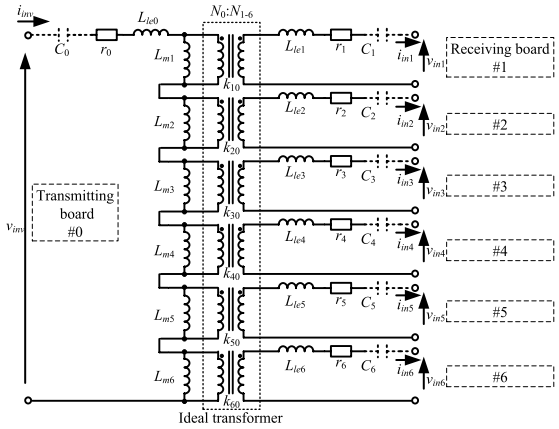

Fig. 5. Equivalent circuit of the proposed isolation system without converters

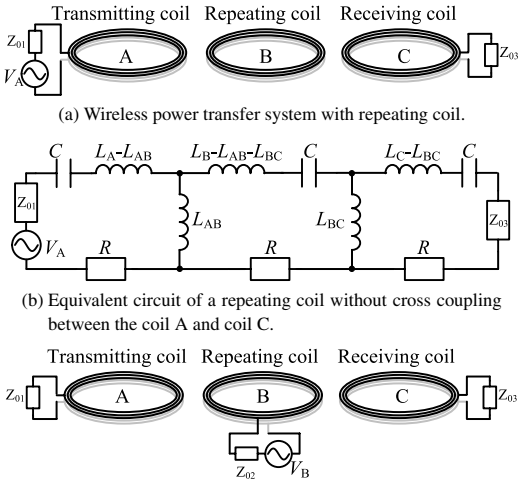

Fig. 6. Equivalent circuit of the wireless power transfer system with a repeater coil [22] and the wireless power transfer system with multiple receivers

multiple receivers is introduced. Because the difference of the wireless power transfer system with a repeating coil and the multiple receivers are only the connection of the power supply. Thus the equivalent circuit of a wireless power transfer system with multiple receivers is shown in Fig. 6(d). It is notable that the magnetizing inductances L_{AB} and L_{BC} are connected in series to the power supply V_B with the inner impedance of Z_{02} in the wireless power transfer system with multiple receivers.

Since the magnetizing inductances are connected in series, the equivalent circuit of the proposed system shown in Fig. 5 is determined. The coil B in Fig. 6(d) corresponds to the transmitting coil #0. The coils A and B correspond to the receiving coils #1-6. The power is transmitted from the transmitting coil to the six receiving coils with the magnetizing inductances, which is connected in series from the view point

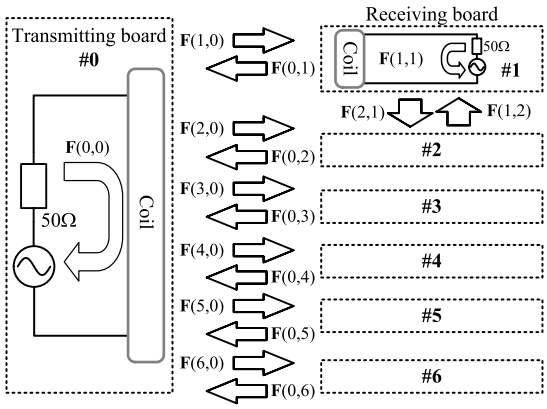

Fig. 7. Definitions of the F-parameter in the isolation system

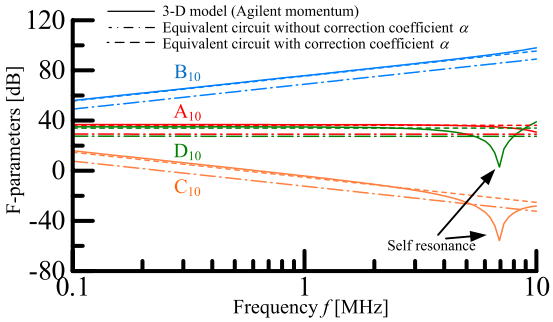

Fig. 8. F-matrix between the transmitting board #0 and receiving board #1

of v_{inv} as shown in Fig. 5.

3.2 Evaluation of the Equivalent Circuit In order to evaluate the validity of the equivalent circuit, the F-matrix (ABCD-matrix) of the frequency characteristics (which is defined by Eq. (1)) analyzed by 3-D electromagnetic analysis (Agilent, Momentum) is compared with the F-matrix calculated by the equivalent circuit. The F-matrix shows the relationship of a system between the input port i and output port j based on voltage and current. The suffixes i and j indicate the number of PCBs (i, $j = 0, 1, \cdots, 6$). For simplicity, the F-parameter from one board #i to another board #j is indicated as $\mathbf{F}(i, j)$.

$$\begin{pmatrix} \dot{V}_i \\ \dot{I}_i \end{pmatrix} = \mathbf{F}(i,j) \begin{pmatrix} \dot{V}_j \\ \dot{I}_j \end{pmatrix} = \begin{pmatrix} A_{ij} & B_{ij} \\ C_{ij} & D_{ij} \end{pmatrix} \begin{pmatrix} \dot{V}_j \\ \dot{I}_j \end{pmatrix} \cdots\cdots\cdots\cdots (1)$$

Figure 7 shows the definitions of the F-parameters in the proposed system. In this evaluation, only the characteristics of the coils are evaluated. Thus, the ideal power supply with resistances of 50 Ω for the inner impedance is connected instead of the converters. The inner impedance is necessary because the F-parameters are calculated from the analysis results of the scattering parameter (S-parameter) by a simulator. Moreover, the resonance capacitors are omitted because the evaluation of the equivalent circuit of the transmission coils is the main purpose of this section.

Figure 8 shows each of the F-parameters between the transmitting board and receiving board #1. The solid line shows the F-parameter analyzed from 3-D electromagnetic analysis. The dashed-dotted line shows the F-parameter calculated from the equivalent circuit. The dotted line shows

$$\dot{I}_{inv} = \frac{\dot{V}_{inv}}{\Delta}\left\{\left(r'_1 + R'_1\right) + j\left(\omega L'_{le1} + \omega L_{m1} - \frac{1}{\omega C'_1}\right)\right\}\left\{\left(r'_2 + R'_2\right) + j\left(\omega L'_{le2} + \omega L_{m2} - \frac{1}{\omega C'_2}\right)\right\}\cdots\left\{\left(r'_6 + R'_6\right) + j\left(\omega L'_{le6} + \omega L_{m6} - \frac{1}{\omega C'_6}\right)\right\} \quad \cdots\cdots (3)$$

$$\Delta = \begin{vmatrix} r_0 + j\left(\omega L_{le0} + \omega L_{m1} + \omega L_{m2} + \cdots + \omega L_{m6} - \frac{1}{\omega C_0}\right) & -j\omega L_{m1} & -j\omega L_{m2} & \cdots & -j\omega L_{m6} \\ -j\omega L_{m1} & \left(r'_1 + R'_1\right) + j\left(\omega L'_{le1} + \omega L_{m1} - \frac{1}{\omega C'_1}\right) & 0 & \cdots & 0 \\ -j\omega L_{m2} & 0 & \left(r'_2 + R'_2\right) + j\left(\omega L'_{le2} + \omega L_{m2} - \frac{1}{\omega C'_2}\right) & \cdots & 0 \\ \vdots & \vdots & \vdots & \ddots & \vdots \\ -j\omega L_{m6} & 0 & 0 & \cdots & \left(r'_6 + R'_6\right) + j\left(\omega L'_{le6} + \omega L_{m6} - \frac{1}{\omega C'_6}\right) \end{vmatrix} \quad \cdots\cdots (4)$$

the F-parameter calculated from the equivalent circuit with correction coefficients, which are mentioned later. The F-parameter with the 3-D electromagnetic analysis has a self-resonance at a frequency of approximately 7 MHz. However, the equivalent circuit model does not consider self-resonance because the self-resonance frequency is far from the operating frequency. This is one of the reasons for the error between 3 MHz and 10 MHz.

Moreover, the F-parameter with the equivalent circuit has offsets of approximately 10 dB between 100 kHz and 3 MHz. The reason for the error is the difference between the numbers of the actual windings and effective windings. This means that a portion of the windings is not effective to induce the voltage. This is a specific problem when a transmitting coil is placed on PCBs. The difference can be corrected using a correction coefficient α. The corrected turn-ratio a' of the transformer is represented as Eq. (2) using the correction coefficient α.

$$a' = \alpha\frac{N_1}{N_2} \quad \cdots\cdots (2)$$

The dotted line shows the F-parameter with the equivalent circuit considering the correction coefficient in Fig. 8. The correction coefficients, which are derived by trial and error, are $\alpha_{1\text{–}6}$ = 2.26, 2.28, 2.27, 2.26, 2.28, and 2.27, respectively, in the prototype. The role of the correction coefficients α is to compensate the difference between the actual number of turns and the effective number of turns. Induced voltages at coils are not proportional to the actual number of turns because the radii of the receiving coils are not constant when a spiral coil is used. Thus a magnetic flux partially interlinks across the receiving coils. It is specific characteristic when a spiral coil without magnetic core is used. For this reason, the correction coefficients are necessary in a time-domain analysis in order to analyze the circuit performance.

The F-parameter of the equivalent circuit considering the correction coefficient shows agreement with one of the electromagnetic analyses between 100 kHz and 3 MHz.

3.3 Design of Resonance Capacitors Figure 9 shows the equivalent circuit of the proposed system with the converters. In the following calculation, the rectifiers are assumed as load resistances $R_{1\text{–}6}$ for simplicity. The resonance capacitors are designed to cancel out the reactance owing to the leakage inductance. From the equivalent circuit, the output current of the inverter is expressed as Eq. (3), where Δ is

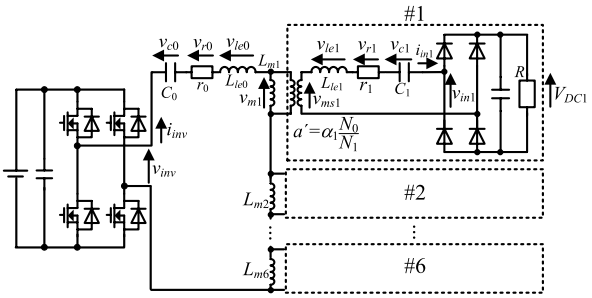

Fig. 9. Equivalent circuit with the power converters

Eq. (4). The prime parameters are the parameters referring to the primary side.

In order to correct the load power factor, the reactance of the Eq. (3) has to be zero. Thus, the resonance conditions are derived as Eqs. (5) and (6), where $\omega = 2\pi f$ is the output angular frequency of the power supply, and $L_{0\text{–}6}$ are the self-inductances of the coils. Equations (5) and (6) indicate that the resonance capacitors should be selected to resonate with each self-inductance because the sum of the resonance leakage inductance and the magnetizing inductances is equal to each self-inductance. This means that the resonance conditions of the isolation system with multiple receivers are the same as those of the isolation system with one receiver.

$$C_0 = \frac{1}{\omega^2\left(L_{le0} + L_{m1} + L_{m2} + \cdots + L_{m6}\right)} = \frac{1}{\omega^2 L_0} \quad \cdots\cdots (5)$$

$$C'_{1\text{–}6} = \frac{1}{\omega^2\left(L'_{le1\text{–}6} + L_{m1\text{–}6}\right)} = \frac{1}{\omega^2 L'_{1\text{–}6}} \quad \cdots\cdots (6)$$

The output current of the inverter is developed with the resonance conditions as Eq. (7) and Eq. (8), which clearly show that the unity input power factor of the load is achieved by the resonance.

$$\dot{I}_{inv}\left(\omega = \omega_{re}\right) = \frac{\dot{V}_{inv}}{\Delta\left(\omega = \omega_{re}\right)}\left(r'_1 + R'_1\right)\left(r'_2 + R'_2\right)\cdots\left(r'_6 + R'_6\right) \quad \cdots\cdots (7)$$

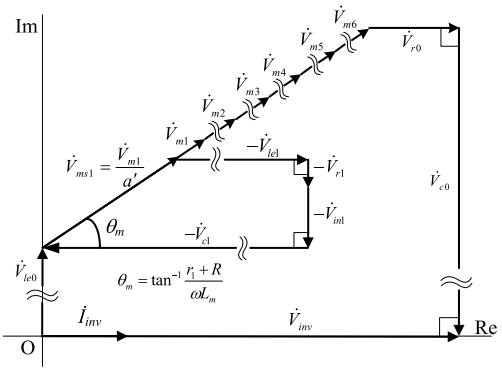

Fig. 10. Vector diagram of the proposed isolation system under the resonance conditions

$$\begin{aligned}\Delta(\omega=\omega_{re}) &= r_0\left(r_1'+R_1'\right)\left(r_2'+R_2'\right)\cdots\left(r_6'+R_6'\right)\\ &+\omega^2L_{m1}^2\left(r_2'+R_2'\right)\left(r_3'+R_3'\right)\cdots\left(r_6'+R_6'\right)\\ &+\omega^2L_{m2}^2\left(r_1'+R_1'\right)\left(r_3'+R_3'\right)\cdots\left(r_6'+R_6'\right)\\ &\vdots\\ &+\omega^2L_{m6}^2\left(r_1'+R_1'\right)\left(r_2'+R_2'\right)\cdots\left(r_4'+R_4'\right)\left(r_5'+R_5'\right)\end{aligned} \quad \cdots\cdots (8)$$

If all of the parameters on the receiving boards and the coupling coefficients are the same, the inverter output current, which is provided by Eq. (3), can be simplified as

$$\dot{I}_{inv} = \frac{\dot{V}_{inv}}{\Delta}\left\{\left(r_1'+R_1'\right)+j\left(\omega L_{le1}'+\omega L_{m1}-\frac{1}{\omega C_1'}\right)\right\}^6 \quad \cdots\cdots (9)$$

where Δ is

$$\begin{aligned}\Delta = &\left\{r_0+j\left(\omega L_{le0}+6\omega L_{m1}-\frac{1}{\omega C_0}\right)\right\}\left\{\left(r_1'+R'\right)+j\left(\omega L_{le1}'+\omega L_{m1}-\frac{1}{\omega C_1'}\right)\right\}^6\\ &+6\omega^2L_m^2\left\{\left(r_1'+R'\right)+j\left(\omega L_{le1}'+\omega L_{m1}-\frac{1}{\omega C_1'}\right)\right\}^5\end{aligned} \quad \cdots\cdots (10)$$

Figure 10 shows the vector diagram under the resonance conditions. For simplicity, all of the parameters on the receiving sides (including the load resistance) are assumed to be the same among the receiving boards. Moreover, the fundamental components are only considered here. The output voltages $V_{in1\text{–}6}$ is expressed by Eq. (11) when all of the parameters on the receiving boards and coupling coefficients are the same. Note that it is effective only when the AC resistance loads are connected to the transmitting coil directly, not the rectifiers.

$$\dot{V}_{in1\text{–}6}(\omega=\omega_{re}) = \frac{j\omega L_{m1}R_1'\left(r_1'+R'\right)^5}{r_0\left(r_1'+R_1'\right)^6+6\omega^2L_{m1}^2\left(r_1'+R_1'\right)^5}\dot{V}_{inv} \quad \cdots\cdots (11)$$

4. Experimental Verifications

4.1 System Setup of the Prototype Figure 11 shows a photograph of the isolation system prototype. The transmitting board, which is shown in Fig. 3, and the receiving boards, which are shown in Fig. 4, are placed as shown in Fig. 2. The chassis is made from acrylic except for clinchers because eddy current losses should be suppressed.

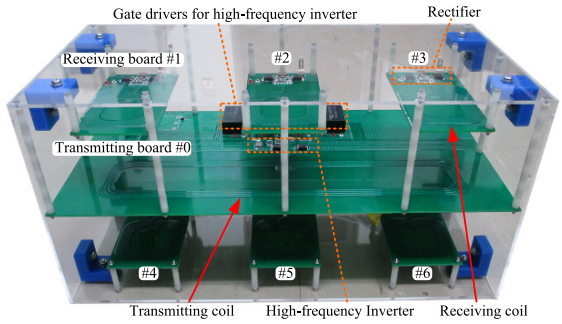

Fig. 11. Prototype of the isolation system

Table 1. Specifications of the prototype

Input voltage (DC)		V_{DC}	24	V
Switching frequency		f_{sw}	2.00	MHz
Self-inductances	Transmitting coil	L_0	20.3	μH
	Receiving coils	$L_{1\text{-}6}$	14.8	μH
Equivalent series resistances	Transmitting coil	R_0	790	mΩ
	Receiving coils	$R_{1\text{-}6}$	690	mΩ
capacitances	Transmitting board #0	C_0	310	pF
	Receiving boards #1-6	$C_{1\text{-}6}$	430	pF
Coupling coefficients (between the receiving coils and transmitting coil)	Receiving board #1	k_{01}	0.017	
	Receiving board #2	k_{02}	0.025	
	Receiving board #3	k_{03}	0.018	
	Receiving board #4	k_{04}	0.017	
	Receiving board #5	k_{05}	0.025	
	Receiving board #6	k_{06}	0.017	

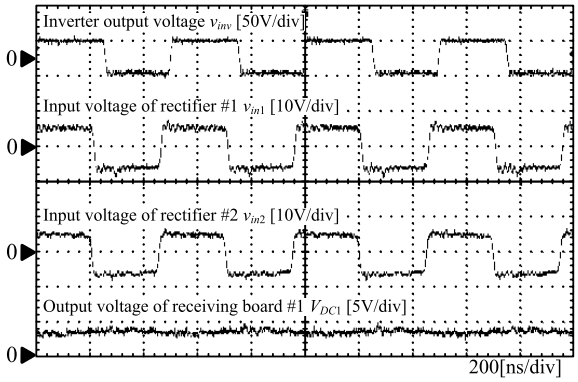

Fig. 12. Operation waveforms of the proposed system with resistance loads of 38 Ω

Table 1 shows the specifications of the prototype. The laminated ceramic capacitors for resonance are selected to satisfy the resonance conditions shown as Eqs. (5) and (6). Note that the coupling coefficients between the boards are simulated values because it is difficult to measure the coupling coefficient accurately.

4.2 Fundamental Characteristics Figure 12 represents the operation waveforms of the proposed isolation system. Note that the resistances of 38 Ω are connected at the outputs of the system instead of the gate drivers for simplicity. The inverter is operated at a frequency of 2.0 MHz. The DC voltages are obtained as the outputs of receiving board

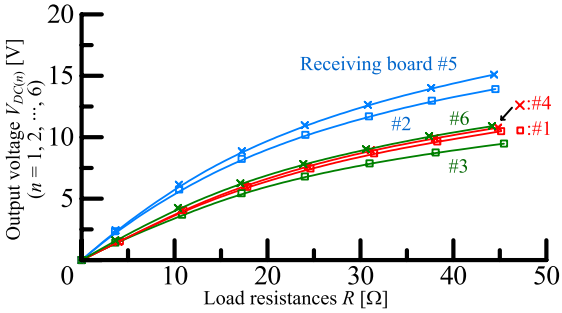

Fig. 13. Output voltage characteristic of the proposed isolation system. The output voltage increases with an increase in load resistance

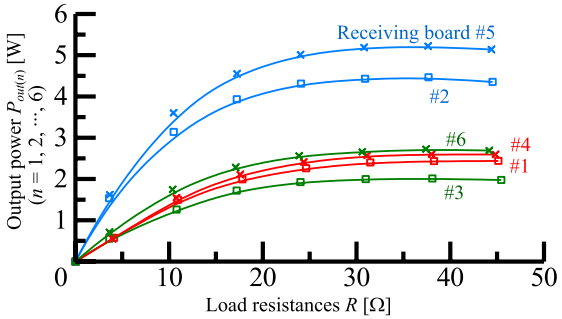

Fig. 14. Output power characteristic of the proposed isolation system

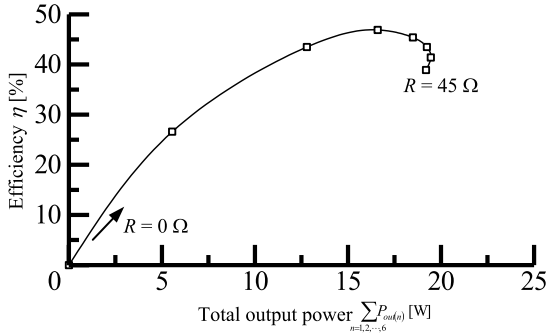

Fig. 15. Measured efficiency characteristic of the proposed system. The same resistance loads are connected to all of the receiving boards as loads

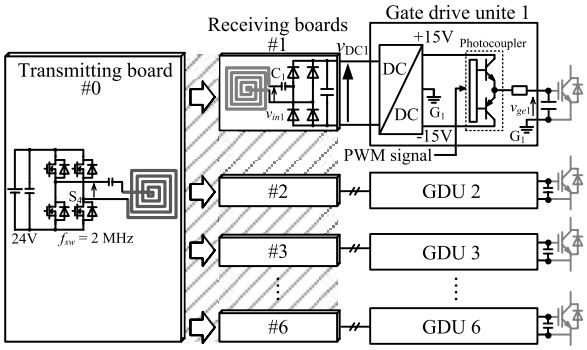

Fig. 16. Experimental setup with gate drivers

#1. The other boards obtained DC voltages, similarly. In theory, the input voltage of v_{in1-6} is 90 degrees phase lead to the inverter output voltage v_{inv} according to Eq. (11). However the phase difference between these voltages is smaller than theoretical calculation. It is caused by the error between the resonance frequency of each board and the transmission frequency because the ceramic capacitors have large tolerances on capacitances. In order to overcome this problem, high-accuracy capacitors with low temperature coefficient should be used.

Figures 13 and 14 show the output voltage and output power characteristic of the proposed isolation system. Each output voltage increases gradually with an increase in load resistance.

The output voltages of the receiving boards #2 and #5 are higher than the others because the coupling coefficients are approximately twice the values of the others. The different coupling coefficients are caused by the positional relationship of the receiving boards. For this reason, the output power is also different with each board. Because the output voltage depends on the load, voltage regulators are necessary in the gate drive circuits.

At light load, the output voltage is too low to drive the voltage regulators. Thus, it is necessary to consume power above a certain level in the gate drive circuit.

Figure 15 represents the measured total efficiency of the proposed system. The total efficiency is defined by Eq. (12), where P_{in} is the input DC power of the isolation system. The total efficiency is the ratio of the input power and the sum of the output power for all of the receiving boards. Note that the same resistance loads are connected to all of the receiving boards as a load.

$$\eta = \frac{\sum_{n=1,2,\cdots,6} P_{out(n)}}{P_{in}} \times 100 \cdots\cdots\cdots\cdots\cdots\cdots\cdots\cdots (12)$$

The maximum efficiency is 46.9% at an output power of 16.6 W. In the isolation system for a medium-voltage inverter, low efficiency can be acceptable because the power loss in the isolation system is considerably smaller than the rated power of a medium-voltage inverter (i.e., 1 MW). Thus, the isolation system is designed to give priority to the isolation performance over the efficiency.

4.3 Operation with Gate Drivers

In this subsection, the prototype with the gate drivers is tested.

Figure 16 shows the experimental setup for the experiments of the proposed isolation system with the gate drivers. The gate drivers (which are operated at a switching frequency of 10 kHz at gate-emitter voltages of ±15 V) and the IGBTs (C_{ge} = 1800 pF) are connected as a load. Note that DC/DC converters are connected as voltage regulators at the front end of the gate drivers. The DC/DC converters output voltages of ±15 V. Moreover, photocouplers are used in order to drive the IGBTs despite the deficient isolation distance because the isolation of the PWM signal is not a main topic of this paper.

Figure 17 shows the operation waveforms with the IGBTs. Even if the gate drivers and IGBTs are connected as a load, the operation system achieves wireless power transfer beyond an air gap of 50 mm.

From the experimental results, it is confirmed that the proposed system can be used as an isolation system for a medium-voltage inverter.

5. Conclusion

A conventional galvanic isolation system for a gate driver

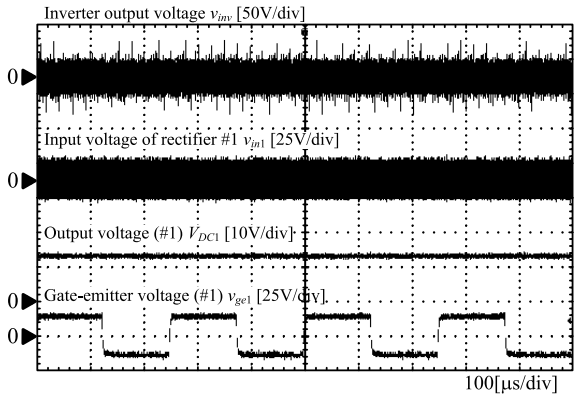

(a) Gate-emitter voltage with proposed isolation system.

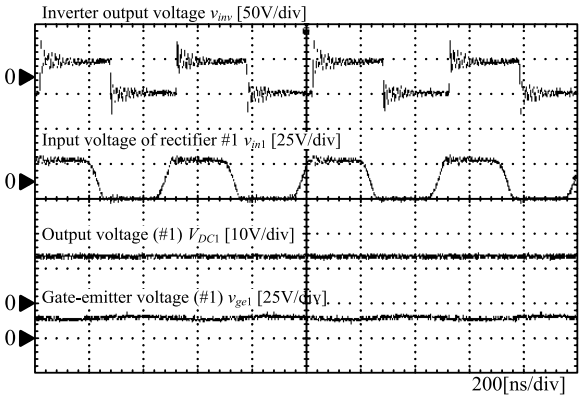

(b) Expanded operation waveforms of (a).

Fig. 17. Operation waveforms of the proposed isolation system with the gate drivers

supply with PCBs has been developed. However, the cost reduction of the conventional system is limited because the transmitting side transmits power to only one receiver.

In this paper, the equivalent circuit of the multiple gate driver supplies using PCBs and resonant conditions were discussed for when the number of receivers increases from one to multiple. The isolation system transmits power from one transmitting board to six receiving boards. Due to this characteristic, the cost of the gate driver supplies can be decreased.

Firstly, an equivalent circuit model was derived and evaluated based on the equivalent circuit of the repeating coil system. It was confirmed that the F-parameters of the equivalent circuit, which has six magnetizing inductance in series in the transmitting side, shows good agreement with the analysis results of 3-D electromagnetic analysis. The resonance conditions are derived based on the introduced equivalent circuit. Then, the isolation system was experimentally demonstrated. Finally, the experimental results showed that the prototype transmits power beyond an air gap of 50 mm using resonance. Moreover, the isolation system achieves a maximum efficiency from an input DC to output DC of 46.9% at a summed output power of 16.6 W.

References

(1) N. Hatti, Y. Kondo, and H. Akagi: "Five-Level Diode-Clamped PWM Converters Connected Back-to-Back for Motor Drives", *IEEE Trans. on Industry Applications*, Vol.44, No.4, pp.1268–1276 (2008)

(2) N. Hatti, K. Hasegawa, and H. Akagi: "A 6.6-kV Transformerless Motor Drive Using a Five-Level Diode-Clamped PWM Inverter for Energy Savings of Pumps and Blowers", *IEEE Trans. on Power Electronics*, Vol.24, No.3, pp.796–803 (2009)

(3) K. Sano and T. Masahiro: "A Transformerless D-STATCOM Based on a Multivoltage Cascade converter Requiring No DC Sources", *IEEE Trans. on Power Electronics*, Vol.27, No.6, pp.2783–2795 (2012)

(4) I. Shigenori and H. Akagi: "A Bidirectional Isolated DC-DC Converter as a Core Circuit of the Next-Generation Medium-Voltage Power Conversion System", *IEEE Trans. Power Electronics*, Vol.22, No.2, pp.535–803 (2009)

(5) S. Dieckerhoff, S. Bernet, and D. Krug: "Power Loss-Oriented Evaluation of High Voltage IGBTs and Multilevel Converters in Transformerless Traction Applications", *IEEE Trans. Power Electronics*, Vol.20, No.6, pp.1328–1336 (2005)

(6) International Electrotechnical Commission (IEC): "Adjustable speed electrical power drive systems—Part 5-1: safety requirements—Electrical, thermal and energy", IEC 61800-5 (2007)

(7) C. Marxgut, J. Biela, J.W. Kolar, R. Steiner, and P.K. Steimer: "DC-DC Converter for Gate Power Supplies with an Optimal Air Transformer", in Proc. Applied Power Electronics Conference and Exposition 2010, pp.1865–1870 (2010)

(8) S. Nagai, N. Negoro, T. Fukuda, N. Otsuka, H. Sakai, T. Ueda, T. Tanaka, and D. Ueda: "A DC-isolated gate drive IC with drive-by-microwave technology for power switching devices", in Proc. International Solid-State Circuits Conference 2012, pp.404–406 (2012)

(9) S. Nagai, T. Fukuda, N. Otsuka, D. Ueda, N. Negoro, H. Sakai, T. Ueda, and T. Tanaka: "A one-chip isolated gate driver with an electromagnetic resonant coupler using a SPDT switch", in Proc. 24th IEEE International Symposium on Power Semiconductor Devices and ICs 2012, pp.73–76 (2012)

(10) S. Nagai, N. Negoro, T. Fukuda, H. Sakai, T. Ueda, T. Tanaka, N. Otsuka, and D. Ueda: "Drive-by-Microwave technologies for isolated direct gate drivers", in Proc. IEEE Microwave Workshop Series on Innovative Wireless Power Transmission: Technologies, Systems, and Applications 2012, pp.267–270 (2012)

(11) M. Ishigaki and H. Fujita: "A Resonant Gate-Drive Circuit for Fast High-Voltage Power Semiconductor Devices with Optical Isolation of Both Control Signal and Power Supply", *IEEJ Trans. IA*, Vol.129, No.3, pp.303–310 (2009) (in Japanese)

(12) R. Steiner, P.K. Steimer, F. Krismer, and J.W. Kolar: "Contactless Energy transmission for an Isolated 100 W Gate Driver Supply of a Medium Voltage Converter", in Proc. Annual Conference of the IEEE Industrial Electronics Society 2009, pp.302–307 (2009)

(13) A. Karalis, J.D. Joannopoulos, and M. Soljacic: "Efficient Wireless non-radiative mid-range energy transfer", Annals of Physics, Vol.323, No.1, pp.34–48 (2007)

(14) S.Y.R. Hui, Y.X. Zhong, and C.K. Lee: "A Critical Review of Recent Progress in Mid-Range Wireless Power Transfer", *IEEE Trans. on Power Electronics*, Vol.29, No.9, pp.4500–4511 (2012)

(15) M. Budhia, G.A. Covic, and J.T. Boys: "Design and Optimization of Circular Magnetic Structures for Lumped Inductive Power Transfer Systems", *IEEE Trans. on Power Electronics*, Vol.26, No.11, pp.3096–3108 (2011)

(16) T. Imura and Y. Hori: "Maximizing Air Gap and Efficiency of Magnetic Resonant Coupling for Wireless Power Transfer Using Equivalent Circuit and Neumann Formula", *IEEE Trans. on Industrial Electronics*, Vol.58, No.10, pp.4746–4752 (2011)

(17) S. Lee and R.D. Lorenz: "Development and Validation of Model for 95%-Efficiency 200-W Wireless Power Transfer Over a 30-cm Air-gap", *IEEE Trans. on Industry Applications*, Vol.47, No.6, pp.2495–2504 (2011)

(18) T. Nakanishi and J. Itoh: "Evaluation of Control Methods for Isolated Three-phase AC-DC converter using Modular Multilevel Converter Topology", in Proc. International Energy Conversion Congress and Exhibition Asia 2013, pp.52–58 (2013)

(19) Z. Tiefu, W. Jun, A.Q. Jun, and A. Agarwal: "Comparisons of SiC MOSFET and Si IGBT Based Motor Drive Systems", in Proc. 42nd IEEE Industry Applications Society Annual Meeting 2007, pp.331–335 (2007)

(20) Infineon: "Datasheet of EiceDRIVER 2ED300C17-S" (2013)

(21) CT-CONCEPT Technologie GmbH: "Datasheet of EiceMELTER 2SD-300C17" (2013)

(22) T. Imura: "Equivalent Circuit for Repeater Antenna for Wireless Power Transfer via Magnetic Resonant Coupling Considering Signed Coupling", in Proc. 6th IEEE Conf. On Industrial Electronics and Applications 2011, pp.1501–1506 (2011)

(23) D. Ahn and S. Hong: "A Study on Magnetic Field Repeater in Wireless Power Transfer", *IEEE Trans. on Industrial Electronics*, Vol.60, No.1, pp.360–371 (2013)

Keisuke Kusaka (Student Member) received his B.S. and M.S. degrees in electrical, electronics and information engineering from Nagaoka University of Technology, Niigata, Japan in 2011 and 2013, respectively. He is currently a Ph.D. candidate at Nagaoka University of Technology, Niigata, Japan. His research interests include an inductive power transfer and a high-frequency power conversion. He is a member of the Institute of Electrical Engineers of Japan, the Institute of Electrical and Electronics Engineers and the Society of Automotive Engineers of Japan.

Koji Orikawa (Member) received his M.S. and Ph.D. degrees in electrical, electronics and information engineering from Nagaoka University of Technology, Niigata, Japan in 2010 and 2013, respectively. Since 2013, he has been working at Nagaoka University of Technology as a postdoctoral fellowship. He is a member of IEEE and IEEJ. His research interests include power conversion system especially DC-DC converters and high frequency techniques for power converters.

Jun-ichi Itoh (Member) received his M.S. and Ph.D. degrees in electrical and electronic systems engineering from Nagaoka University of Technology, Niigata, Japan in 1996 and 2000, respectively. From 1996 to 2004, he was with Fuji Electric corporate Research and Development Ltd., Tokyo, Japan. Since 2004, He has been with Nagaoka University of Technology as an associate professor. He received the IEEJ academic promotion award (IEEJ Technical Development Award) in 2007 and the Isao Takahashi power electronics award in 2010. His research interests include matrix converters, DC/DC converters, power factor correction techniques and motor drives. He is a member of the Institute of Electrical Engineers of Japan and the Society of Automotive Engineers of Japan.

Isamu Hasegawa (Non-member) is currently a Power Electronics R&D Engineer with the MEIDENSHA CORPORATION.

Kazunori Morita (Member) is currently a Power Electronics R&D Engineer with the MEIDENSHA CORPORATION.

Takeshi Kondo (Non-member) is currently a Power Electronics R&D Engineer with the MEIDENSHA CORPORATION.